Giftet Inc.
Journal of Geolocation, Geo-information, and Geo-intelligence
Volume 2015, article ID 2015082105, 13 pages
https://doi.org/10.18610/JG3.2015.082105

Technical Report

VBOC1(α) and VBOC2(α,1−α) Generalized Multi-dimensional Geolocation Modulation Waveforms — Technical Report

Ilir F. Progri[1]

[1]*Giftet Inc., 5 Euclid Ave. #3, Worcester, MA 01610, USA*

Correspondence should be addressed to Ilir Progri; iprogri@giftet.com

Received December 8, 2013; Revised December 19, 21, 2013-January 7, 2014, March 12, 17, 2014, May 31-August 29, 2014 Presented September 18, 2015, Accepted August 21, 2015; Published November 1, 2015.

This technical report provides the results obtained from first original and complete mastery of treatment of Variable Binary Offset Carrier VBOC1(α) and VBOC2(α,1-α) generalized multidimensional geolocation modulation waveforms, to improve the standardization of geolocation waveforms of the United States DoD GPS, European Galileo, Russian GLONASS, Chinese Compass, Indian IRNSS in the L-band (1-2 GHz), and the United Nations International Telecommunications Union (ITU) in the S-band (2-4 GHz) and C-band (4-8 GHz).

The main motivation for this technical report is twofold: (a) an illustration of the improved system description or GNSS and Global Precipitation Measurement (GPM) constellation and (b) significantly improved 2-D and 3-D autocorrelation function (ACF) and power spectral density (PSD) results.

Index Terms—Pulse generation, pulse amplitude modulation, pulse width modulation, multidimensional sequences, signal design, signal analysis, generalized functions, time-frequency analysis, minimization methods, optimization methods.

1 Introduction

The main objective of this technical report is the description of $VBOC1(\alpha)$ [1], [2] and $VBOC2(\alpha, 1-\alpha)$ [3], [4] generalized multidimensional geolocation modulation waveforms—results so as to illustrate originality, novelty (or innovation), advancement, and accuracy in signal design and optimization to improve the standardization of geolocation waveforms of the United States DoD GPS, European Galileo, Russian GLONASS, Chinese Compass, Indian IRNSS in the L-band (1-2 GHz), and the United Nations ITU in the S-band (2-4 GHz) [1], [25], C-band (4-8 GHz) [1], [26].

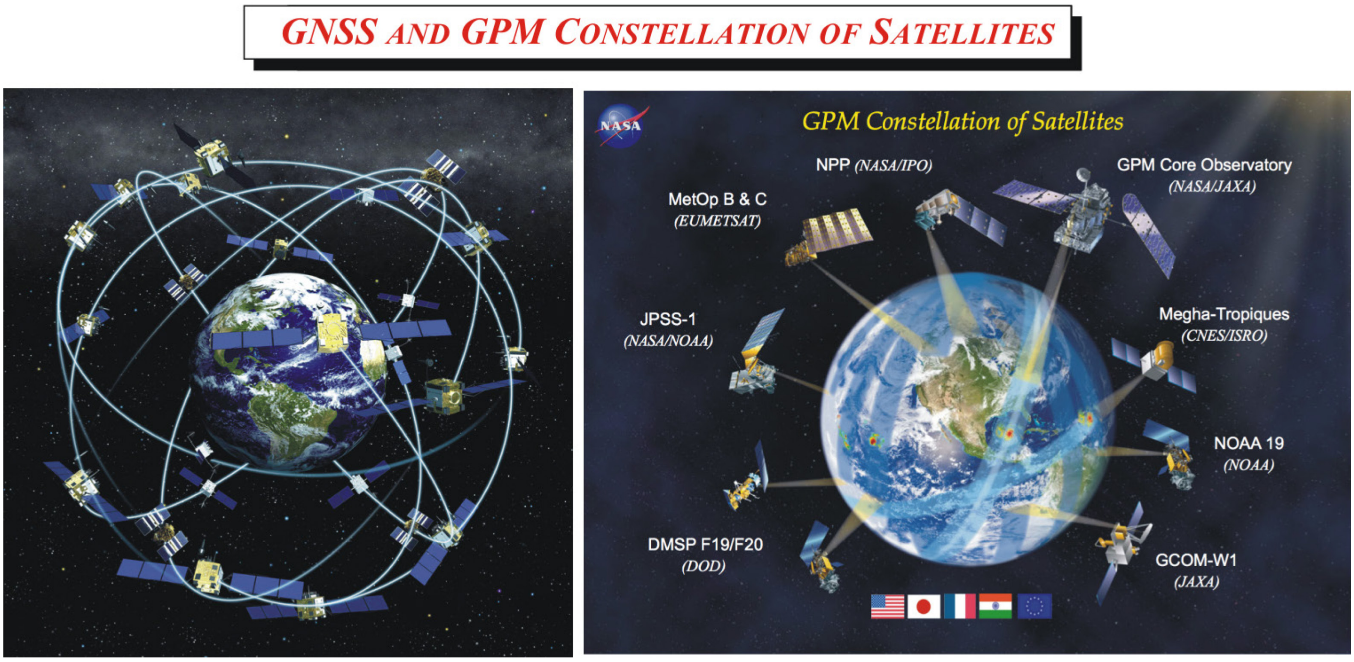

FIGURE 1: GNSS and GPM constellation of satellites.

"*I believe the future of Global Navigation Satellite Systems (GNSS) and particularly GPS will only be limited by our ingenuity and imagination. In terms of economic benefit, GPS contributes $60 billion to our economy, and that's no stretch considering the positive and real advantages GPS affords us every day through fuel savings, transportation optimization, banking transactions, recreational activities, and certainly the defense of our great nation*" [7]—Col. Bernie Gruber.

This technical report illustrates the results of a few examples on how our ingenuity and imagination can be employed to improve GPS (and GNSS) signal design and optimization and offer the GNSS and ITU community at large a significantly improved methodology to resolve any architecture or geolocation standardization issues.

Let us compare and contrast, in a sequential order, the main contributions of this technical report to the ones that have already been published [6]-[37].

First, for the first time asymmetrical VBOC modulations in [8] were published in 2007 and then results of improved VBOC generalized multidimensional geolocation modulation waveforms in 2012 in [6], and the one that is coming in 2014 or 2015 [5]; however, the results shown in this technical report are not published anywhere else.

It is of no surprise that Betz, the inventor of BOC modulation [14], in 2013 [8] suggested that two most important possible changes to future GNSS signals will include asymmetrical and generalized AltBOC spreading modulation and asymmetrical and generalized AltBOC, optimized M-ary constant-envelope for multiplexing.

This technical report addresses exactly what is needed to the GNSS signal design and optimization community, the originality, novelty (or innovation), advancement, and accuracy in signal design and optimization namely $VBOC1(\alpha)$ in [1], [2] and $VBOC2(\alpha, 1-\alpha)$ in [3], [4] that have never been discussed and simulated [6]-[37] to the extent shown in this technical report.

Second, although simulation results discussed here employ certain signal modulation such as C-CDMA, MC-CDMA discussed in [5]-[8], [31]- [37]; here it is shown 3-D ACF and PSD simulation results that have never been presented before.

It was shown both analytically that for $VBOC1(\alpha)$ in [1], [2] and for $VBOC2(\alpha, 1-\alpha)$ in [3], [4] optimum $\alpha = \{0.5, [5/12, 13/29)\}$ respectively, the next task was to show typical time and frequency domain simulation results which include: (1) C-CDMA in S2-band 3.5-3.75 GHz I/Q channel is $VBOC1(\alpha = 0.5)$ / $VBOC2(\alpha = 5/12, 1-\alpha = 7/12)$ and (2) MC-CDMA in C2-band 7-7.5 GHz for which the I/Q channel is $VBOC1(\alpha = 0.5)$ / $VBOC2(\alpha = 0.42, 1-\alpha = 0.58)$ because it was shown that for these values of α we have 94 % efficiency of $VBOC2$ in terms of out-of-phase ACF vs. BOC modulation.

The final set of the simulation results is designed to show the 3-D ACF and PSD as a function of α for $0 \leq \alpha \leq 1$. Why are these simulation results so significant? The significance of these simulation results is: (1) their originality, novelty (or innovation), advancement, and accuracy in signal design and optimization namely $VBOC1(\alpha)$ in [1], [2] and $VBOC2(\alpha, 1-\alpha)$ in [3], [4]; (2) illustration of optimum α for $VBOC1(\alpha = 0.5)$ and $VBOC2(\alpha = 5/12, 1-\alpha = 7/12)$.

This paper is organized as follows: in Sect. 2 system description is given or discussed. Sect. 3 contains simulation results; Conclusion is provided in Sect. 4 along with a list of references.

2 System Description

Davis [10] summarizes a series of proposals, presentations, and discussions as to the Air Force proposed dramatic redesign of GPS constellation based on four requirements: (1) lowering the strict integrity standards; (2) downsizing the GPS constellation by using the so-called NavSats; (3) populating the GPS constellation with NibbleSats; and (4) final progress report is still not yet available [6].

A dramatic redesigned GNSS and Global Precipitation Measurements (GPM) constellation is illustrated in Figure 1.

GNSS constellation is made of GPS, GLONASS, Galileo, Compass, and IRNSS satellites. It is hoped that substantial improvements of the signal design will result in reduction of the power requirements by a factor of two or more; hence, reducing the size and the overall cost for maintaining the GNSS constellation.

The GPM constellation is made of GPM/Core Observatory (NASA/JAXA), Megha-Tropiques (CNES/ISRO), NOAA 19 (NOAA), GCOM-W1 (JAXA), DMSP F19/F20 (DOD), JPSS-1 (NASA/NOAA), MetOp B&C (EUMETSAT), NPP (NASA/IPO).

It is hoped that substantial improvements of the GNSS signal design will result in (1) the reduction of the power requirements of the GPM constellation by a factor of two or more; hence, reducing the size and the overall cost for maintaining the GPM constellation; (2) in improvements of Precipitation Processing System (PPS) at NASA Goddard Space Flight Center, as well as at the JAXA facility in Japan.

Substantial improvements of the GPM constellation will result in substantial improvements of the GNSS channel modeling and GNSS measurements; hence, more accurate GNSS user segment.

This concluded the discussion on system description.

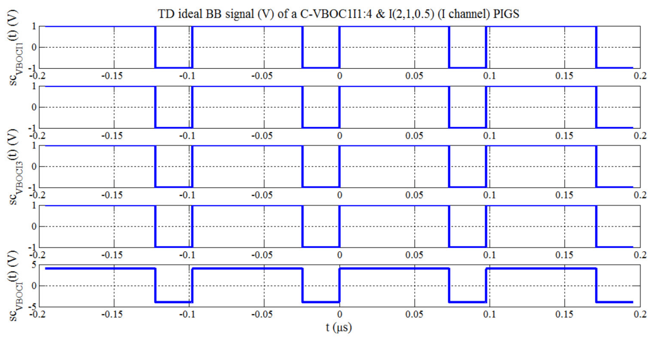

FIGURE 2: 0.4-µs TD BB signal of a *C-VBOC*1I1:4$_{(2,1,0.5)}$ and *VBOC*1I$_{(2,1,0.5)}$, (I channel) PIGS.

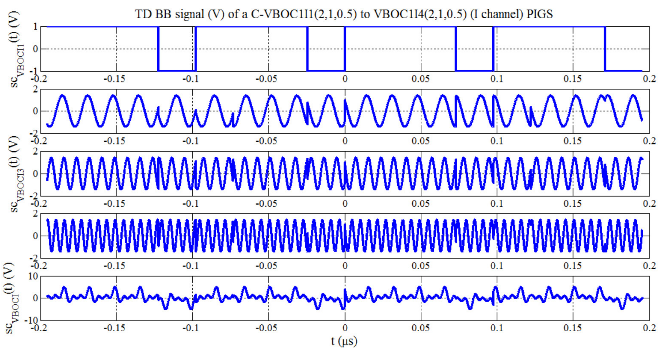

FIGURE 3: 0.4-µs TD BB signal of a *C-VBOC*1I1:4$_{(2,1,0.5)}$ and *VBOC*1I$_{(2,1,0.5)}$, (I channel) PIGS.

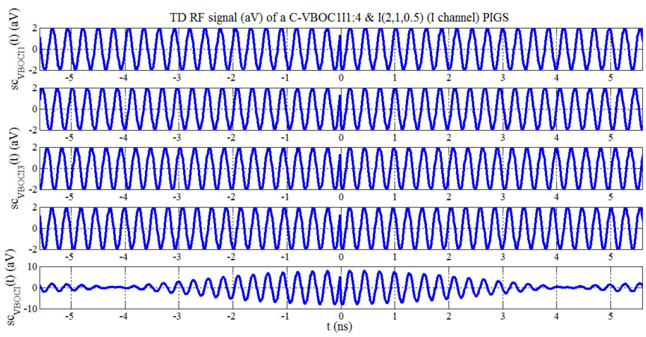

FIGURE 4: 12-ns RF BB signal of a *C-VBOC*1I1:4$_{(2,1,0.5)}$ and *VBOC*1I$_{(2,1,0.5)}$, (I channel) PIGS.

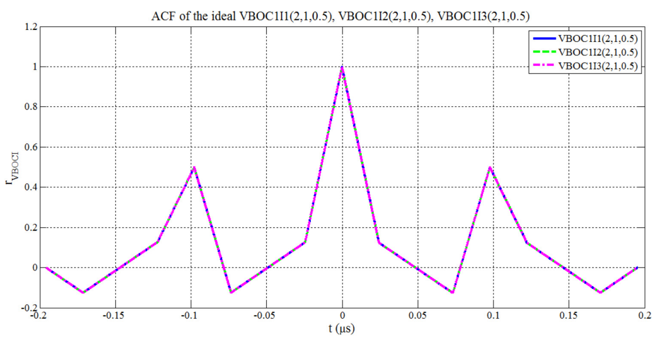

FIGURE 5: 0.4-µs ACF I Ch: *VBOC*1I1:3$_{(2,1,0.5)}$ PIGS.

3 Simulation Results

One efficient way of achieving substantial improvements of the GNSS signal design is by means of the generalized multidimensional geolocation modulation waveforms such as $VBOC1(\alpha)$ and $VBOC2(\alpha, 1-\alpha)$ whose properties are discussed in great detail in [1]-[4].

An original set of very accurate simulation results on $VBOC1(\alpha)$, $VBOC2(\alpha, 1-\alpha)$ ACFs/PSDs are presented in Chap. 7 of [5] and in [6].

However, based on detailed discussion on optimum α; i.e., the simulation results of the optimization theorems 6 of [2], 4 and 5 of [4]; corollaries 5 and 6 of [2] and 2 and 3 [4]; simulation results with optimum $\alpha = [5/12, 13/29)$ $VBOC2_{(2n,n,\alpha)}$ and $VBOC2_{(4n,n,\alpha)}$ are unique and original to this technical report that the reader cannot find in [5], [6].

Simulation results are grouped into two categories: (1) typical time and frequency domain simulation results; and (2) 3-D ACF and PSD simulation results.

3.1 Typical Time and Frequency Domain Simulation Results

Typical time and frequency domain simulation results include: (1) C-CDMA simulation results in S2-band 3.5-3.75 GHz and (2) MC-CDMA simulation results in C2-band 7-7.5 GHz.

3.1.1 C-CDMA Simulation Results in S2-band 3.5-3.75 GHz

Figure 2 illustrates the 0.4-μs TD reference baseband (BB) signal of a $C\text{-}VBOC1I1{:}4_{(2,1,0.5)}$ and $VBOC1I_{(2,1,0.5)}$, (I channel) PIGS. As shown in Figure 2 there are five TD BB waveforms: the first four corresponding to the individual transmitters and the fifth waveform corresponds to the sum waveform: i.e., the sum waveform of the four individual transmitter waveforms. All the four individual transmitter waveforms have a subcarrier frequency equal to zero Hz. The chipping rate is 5,115 MHz. The signal design waveform modulation is the same for all four transmitter waveforms. VBOC type is I or the first VBOC, $m = p = 2, n = 1, \alpha = 0.5$: there are two subcarrier periods for every code chip (or transition) equal to 1.955 μs. For every signal subcarrier the $+1$ time is equal to 0.733125 μs and the -1 time is equal to 0.244375 μs; i.e., half period of the subcarrier is equal to 0.48875 μs. Figure 2 illustrates two periods or chips or code

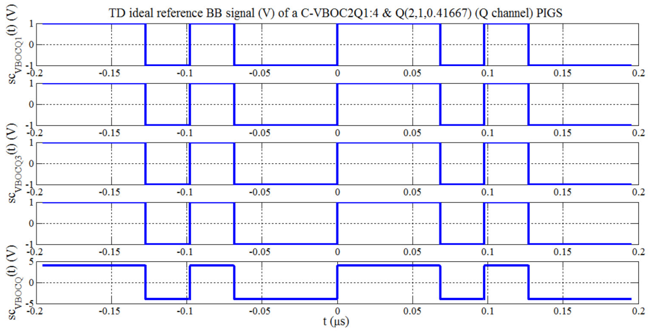

FIGURE 6: 0.4-μs TD BB signal of a $C\text{-}VBOC2Q1{:}4_{(2,1,5/12)}$ and $VBOC2Q_{(2,1,5/12)}$, (Q channel) PIGS.

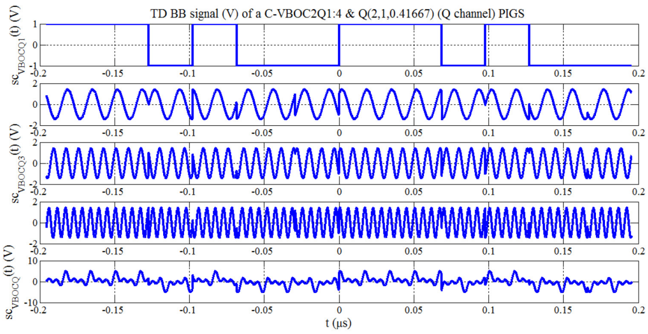

FIGURE 7: 0.4-μs TD BB signal of a $C\text{-}VBOC2Q1{:}4_{(2,1,5/12)}$ and $VBOC2Q_{(2,1,5/12)}$, (Q channel) PIGS.

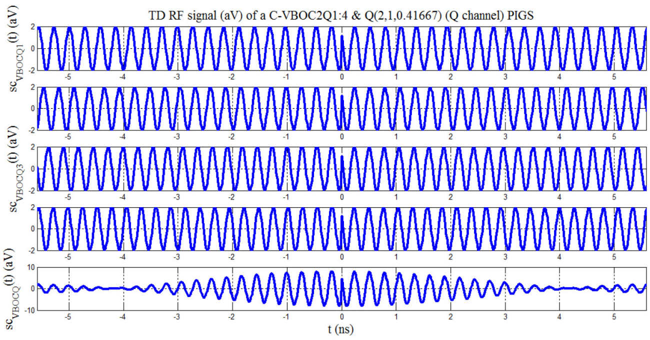

FIGURE 8: 1.2-ns TD RF signal of a $C\text{-}VBOC2Q1{:}4_{(2,1,5/12)}$ and $VBOC2Q_{(2,1,5/12)}$, (Q channel) PIGS.

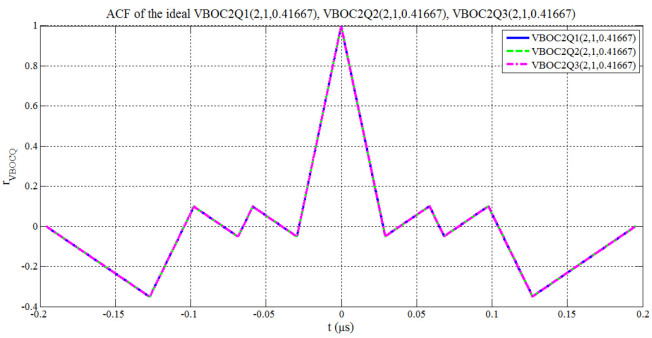

FIGURE 9: 0.4-μs ACF Q Ch:$VBOC2Q1_{(2,1,5/12)}$ PIGS.

transitions of the reference BB signal equal to 3.91 μs or 0.9775×4 μs.

Figure 3 illustrates the 0.4-μs TD BB signal of a $C\text{-}VBOC1I1{:}4_{(2,1,0.5)}$ and $VBOC1I_{(2,1,0.5)}$, (I channel) PIGS. Of the four individual transmitter waveforms the top waveform has a subcarrier frequency equal to zero Hz. The second, third, and fourth subcarrier frequencies are 60, 120, and 180 MHz respectively, which is the reason why this type of signal modulation is known as SC-CDMA or C-CDMA. The chipping rate is 5,115 MHz.

The signal design waveform modulation is the same for all four transmitter waveforms $C\text{-}VBOC1I_{(2,1,0.5)}$; i.e., VBOC type is I or the first VBOC, $m = p = 2$, $n = 1$, $\alpha = 0.5$: with other signal parameters same as in Figure 2.

Figure 4 illustrates the 12-ns TD RF signal of a $C\text{-}VBOC1I1{:}\,4_{(2,1,0.5)}$ and $VBOC1I_{(2,1,0.5)}$, (I channel) PIGS. Figure 4 depicts waveforms of Figure 3 up-converted in the S2-band 3.5-3.75 GHz and because the carrier frequency is so high only the first chip transition is shown

Figure 5 presents the 0.4-μs ACF signal, $r_{VBOC1I1:3_{(2,1,0.5)}}$, of a $C\text{-}VBOC1I1{:}\,3_{(2,1,0.5)}$, and $VBOC1I_{(2,1,0.5)}$, (I channel) PIGS. We can see how much the out-of-phase autocorrelation peaks are reduced which is exactly the reason why $VBOC1I1{:}\,3_{(2,1,0.5)}$ has superior properties compared to $BOC_{(2,1)}$ [5], [6]. We can see that out-of-phase autocorrelation peaks for $VBOC1I1{:}\,3_{(2,1,0.5)}$ do not exceed 0.5 as opposed to the out-of-phase autocorrelation peaks for $BOC_{(2,1)}$ come as close as -0.75 [5], [6].

Figure 6 waveforms parameters are identical to those of Figure 2 with the only difference the signal design modulation: $VBOC2Q_{(2,1,5/12)}$; i.e., VBOC type is II or the second VBOC, $m = p = 2$, $n = 1$, $\alpha = 5/12$. There are two subcarrier periods for every code chip (or transition) equal to 1.955 μs. For every odd signal subcarrier the $+1$ time is equal to 0.68425 μs and the -1 time is equal to 0.29325 μs; i.e., half period of the subcarrier is equal to 0.48875 μs; and for even signal subcarrier the $+1$ time is equal to 0.29325 μs and the -1 time is equal to 0.68425 μs. Figure 6 illustrates two periods or chips or code transitions of the BB signal equal to 3.91 μs or 0.9775×4 μs.

Figure 7 waveforms parameters are identical to those of Figure 3 with the only difference the signal design modulation: $VBOC2Q_{(2,1,5/12)}$; i.e., with other signal parameters identical to those of Figure 6.

Figure 8 displays the 12-ns TD RF signal of a $C\text{-}VBOC2Q1{:}\,3_{(2,1,5/12)}$ and $VBOC2Q_{(2,1,5/12)}$, (Q channel) PIGS. Figure 8 depicts waveforms of Figure 7 up-converted in the S2-band 3.5-3.75 GHz and because the carrier frequency is so high only the first chip transition is shown.

Figure 9 shows the 0.4-μs Q Ch: $VBOC2Q1{:}\,3_{(2,1,5/12)}$ PIGS. We can see how much the out-of-phase autocorrelation peaks are reduced which is exactly the reason why $VBOC2Q1{:}\,3_{(2,1,5/12)}$ has superior properties compared to $VBOC1I1{:}\,3_{(2,1,0.5)}$. We can see that out-of-phase autocorrelation peaks for $VBOC2Q1{:}\,3_{(2,1,5/12)}$ do not exceed -0.35 as opposed to the out-of-phase autocorrelation peaks for $VBOC1I1{:}\,3_{(2,1,0.5)}$ come as close as 0.5.

The $VBOC2_{(2,1,\alpha)}$ type of modulation reduces the out-of-phase autocorrelation peaks by almost half compared to $VBOC1_{(2,1,\alpha)}$ while at the same time offering a very simple waveform modification. Moreover, the phase of the out-of-phase autocorrelation peaks for $VBOC2_{(2,1,\alpha)}$ is different from the phase of the out-of-phase autocorrelation peaks for $VBOC1_{(2,1,\alpha)}$; i.e., when there is an out-of-phase autocorrelation peak for $VBOC2_{(2,1,\alpha)}$ there is a minimum value of the out-of-phase autocorrelation peaks for $VBOC1_{(2,1,\alpha)}$ and vice versa. Therefore, not only does this type of modulation reduces the number of the out-of-phase autocorrelation peaks but it also offsets them as a function of the type of the VBOC modulation and the parameter of the signal design modulation α.

Figure 10 illustrates the 62.5-MHz FD reference BB PSD I Ch: $VBOC1I1{:}\,4_{(2,1,0.5)}$, Q Ch: $VBOC2Q1{:}\,4_{(2,1,5/12)}$ PIGS. Pretty much the same comments can be made for PSD of $VBOC2Q1{:}\,4_{(2,1,5/12)}$ in contrast to PSD shown in Fig. 52 [6]; i.e., the PSD of $VBOC2Q1{:}\,4_{(2,1,5/12)}$ is a much quasi-flatter waveform than the PSD of $VBOC2Q1{:}\,4_{(2,1,0)} = BOC_{(2,1)}$. All waveforms are centered at 0 MHz. The minimums for $VBOC1I1{:}\,4_{(2,1,0.5)}$ are at 5, 15, 25, and 35 MHz. Contrast with the minimums for PSD of $VBOC2Q1_{(2,1,5/12)}$ are at 7, 25, 27, and 31 MHz which is the reason why PSD of $VBOC2Q1{:}\,4_{(2,1,5/12)}$ has a quasi-flatter spectrum as expected. The maximum values for the PSD of $VBOC2Q1{:}\,4_{(2,1,5/12)}/VBOC1I1{:}\,4_{(2,1,0.5)}$ are $-72/-78$ dB respectively.

Figure 11 displays the 250-MHz FD BB PSD of a $C\text{-}VBOC1I1{:}\,4_{(2,1,0.5)}$, (I channel) and $VBOC2Q1{:}\,4_{(2,1,5/12)}$ (Q channel) PIGS. As illustrated in Figure 10 there are four $VBOC1I1{:}\,4_{(2,1,0.5)}$ PSD in the I channel orthogonal with four $VBOC2Q1{:}\,4_{(2,1,5/12)}$ in the Q channel. There are, however, four transmitters hence every *i*th transmitter contains one $VBOC1Ii_{(2,1,0.5)}$, for $i = \{1,2,3,4\}$, i : the transmitter index,

PSD in the I channel orthogonal with one $VBOC2Qi_{(4,1,5/12)}$ PSD, for $i = \{1,2,3,4\}$, i : the transmitter index, in the Q

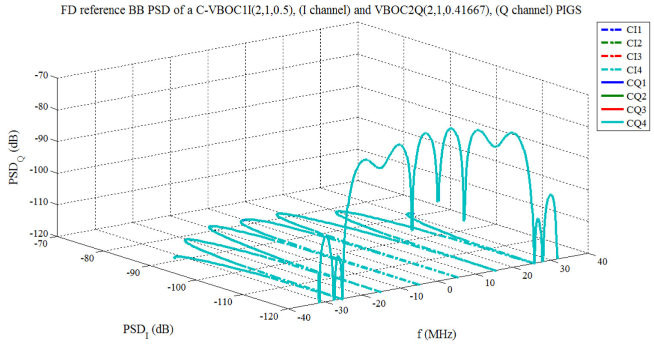

FIGURE 10: 62.5-MHz FD BB PSD of a $C\text{-}VBOC1I_{(2,1,0.5)}$, (I channel) and $VBOC2Q_{(2,1,5/12)}$ (Q channel) PIGS.

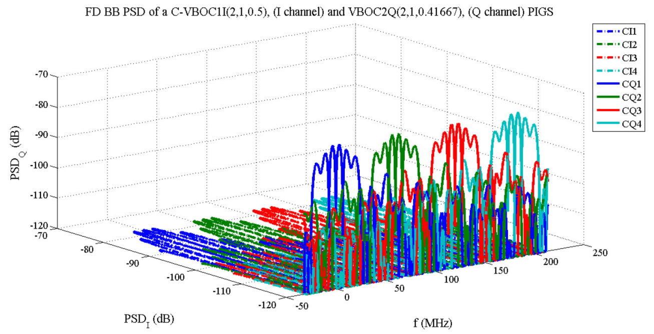

FIGURE 11: 250-MHz FD BB PSD of a $C\text{-}VBOC1I_{(2,1,0.5)}$, (I channel) and $VBOC2Q_{(2,1,5/12)}$ (Q channel) PIGS.

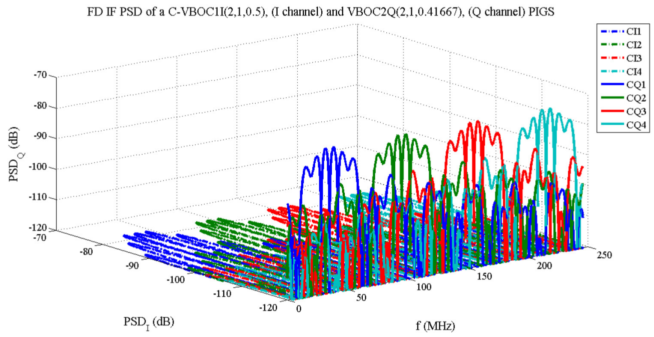

FIGURE 12: 250-MHz FD IF PSD of a $C\text{-}VBOC1I_{(2,1,0.5)}$, (I channel) and $VBOC2Q_{(2,1,5/12)}$ (Q channel) PIGS.

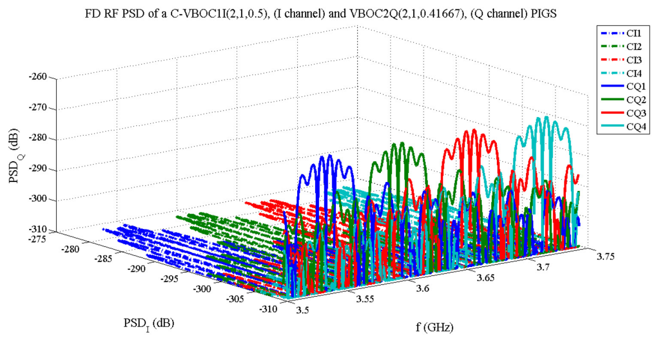

FIGURE 13: 250-MHz FD RF PSD of a $C\text{-}VBOC1I_{(2,1,0.5)}$, (I channel) and $VBOC2Q_{(2,1,5/12)}$ (Q channel) PIGS the S2-band 3.5-3.75 GHz.

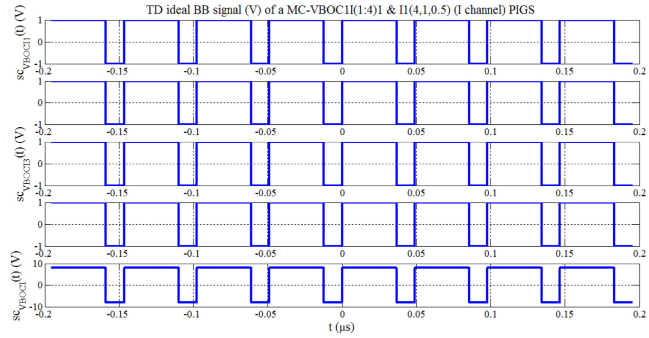

FIGURE 14: 0.4-µs TD ideal reference BB signal of a $MC\text{-}VBOC1I(1{:}4)1_{(4,1,0.5)}$ and $VBOC1I_{(4,1,0.5)}$ PIGS.

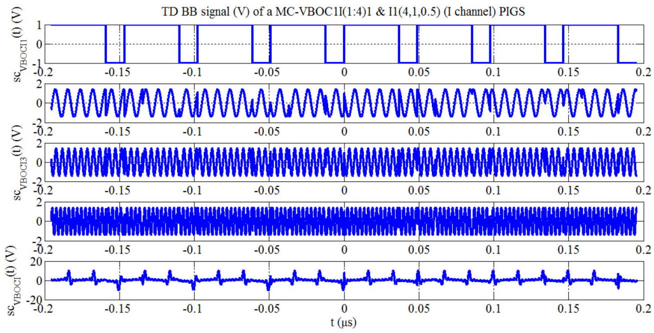

FIGURE 15: 0.4-µs TD BB signal of a $MC\text{-}VBOC1I(1{:}4)1_{(4,1,0.5)}$ and $VBOC1I_{(4,1,0.5)}$ PIGS.

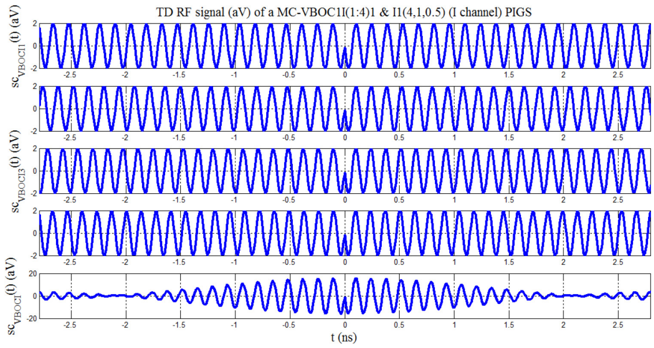

FIGURE 16: 5.5-ns RF BB signal of a $MC\text{-}VBOC1I(1{:}4)1_{(4,1,0.5)}$ and $VBOC1I_{(4,1,0.5)}$ PIGS.

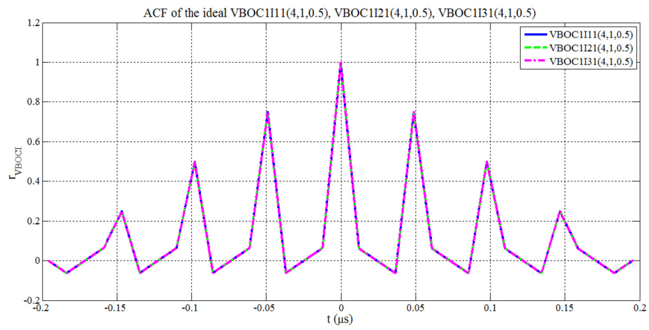

FIGURE 17: 0.4-µs ACF I Ch: $VBOC1I(1{:}3)1_{(4,1,0.5)}$, PIGS.

channel which is the reason why this type of signal modulation is known as single-carrier CDMA or SC-CDMA or C-CDMA. The total BB signal bandwidth is 250 MHz which is results from 62.5 MHz, the signal bandwidth of either $VBOC1I_{(2,1,0.5)}$ or $VBOC2Q_{(2,1,0.4)}$ waveform, times four. The maximum values for the PSD for $VBOC2Q1:4_{(2,1,5/12)}/VBOC1I1:4_{(2,1,0.5)}$ are $-72/-78$ dB respectively.

Figs. 12 and 13 depict the 250-MHz FD IF/RF PSD of a *C*-$VBOC1I_{(2,1,0.5)}$, (I channel) and $VBOC2Q_{(2,1,5/12)}$ (Q channel) PIGS. The waveforms shown in Figure 12 are exactly the same as the ones shown in Figure 11; however, the only difference is that their IF frequency is shifted in by 35 MHz.

Figure 13 shows the 250-MHz FD RF PSD of a *C*-$VBOC1I_{(2,1,0.5)}$, (I channel) and $VBOC2Q_{(2,1,5/12)}$ (Q channel) PIGS the S2-band 3.5-3.75 GHz. The waveforms shown in Figure 13 are exactly the same as the ones shown in Figure 12; however, the only difference is that their carrier frequency is shifted in by 3.5 GHz.

This concludes the summary of $VBOC2Q_{(2,1,5/12)}/VBOC1I_{(2,1,0.5)}$ the C-CDMA simulation results in S2-band 3.5-3.75 GHz in which we have illustrated: (1) the waveforms in TD and FD; and (2) ACF in TD and PSD FD.

3.1.2 MC-CDMA Simulation Results in C2-band 7-7.5 GHz

Figs. 14 through 25 are original plots shown for the first time in an ION technical report.

Figure 14 shows the 0.4-μs ideal TD reference BB signal of a *MC*-$VBOC1I(1:4)1_{(4,1,0.5)}$, and $VBOC1I_{(4,1,0.5)}$, (I channel) PIGS.

As shown in Figure 14 there are five TD BB waveforms: the first four corresponding to the first subcarrier of the individual transmitters and the fifth waveform corresponds to the sum waveform: i.e., the sum waveform of the eight individual transmitter waveforms.

All four individual transmitter waveforms the top waveform has a subcarrier frequency equal to zero Hz. The chipping rate is 5,115 MHz. The signal design waveform modulation is the same for all eight transmitter waveforms C-$VBOC1I_{(4,1,0.5)}$; i.e., VBOC type is I or the first VBOC, $m = p = 4$, $n = 1$, $\alpha = 0.5$: there are four subcarrier periods for every code chip (or transition) equal to 1.955 μs. For every signal subcarrier the $+1$ time is equal to 0.3665625 μs and the -1 time is equal to 0.1221875 μs; i.e., period of the subcarrier is equal to 0.48875 μs. Figure 14 illustrates two periods or chips or code transitions of the BB signal equal to 3.91 μs or 0.48875×8 μs.

Figure 15 illustrates the 0.4-μs TD BB signal of a *MC*-$VBOC1I(1:4)1_{(4,1,0.5)}$, and $VBOC1I_{(4,1,0.5)}$, (I channel) PIGS. Of the four individual transmitter waveforms the top waveform has a subcarrier frequency equal to zero Hz. The second, third, and fourth subcarrier frequencies are 60, 120, and 180 MHz respectively, which is the reason why this type of signal modulation is known as MC-CDMA. Other signal parameters are the same as those in Figure 14.

Figure 16 illustrates the 5.5-ns RF BB signal of a *MC*-$VBOC1I(1:4)1_{(4,1,0.5)}$ and $VBOC1I_{(4,1,0.5)}$, (I channel) PIGS. Figure 16 depicts waveforms of Figure 15 up-converted in the C2-band 7-7.5 GHz and because the carrier frequency is so high only the first chip transition is shown and data up to 5.5 ns; hence, we see no other transition in this very tiny segment.

Figure 17 shows the 0.4-μs ACF I Ch: $VBOC1I1_{(4,1,0.5)}$. We can see how much the out-of-phase autocorrelation peaks are reduced which is exactly the reason why $VBOC1I1_{(4,1,0.5)}$ has superior properties compared to $BOC_{(4,1)}$. We can see that out-of-phase autocorrelation peaks for $VBOC1I1_{(4,1,0.5)}$ do not exceed 0.75 as opposed to the out-of-phase autocorrelation peaks for $BOC_{(4,1)}$ come as close as 0.95.

The $VBOC1_{(4,1,\alpha)}$ type of modulation reduces the out-of-phase autocorrelation peaks by almost half compared to $BOC_{(4,1)}$ while at the same time offering a very simple waveform modification. Moreover, the phase of the out-of-phase autocorrelation peaks for $VBOC1_{(4,1,\alpha)}$ are the same as the phase of the out-of-phase autocorrelation peaks for $BOC_{(4,1)}$.

Figure 18 presents the 0.4-μs TD reference BB signal of a *MC*-$VBOC2Q(1:4)1_{(4,1,0.42)}$ and $VBOC2Q_{(4,1,0.42)}$, (Q channel) PIGS. Figure 18 waveforms parameters are identical to those of Figure 14 with the only difference the signal design modulation: $VBOC2Q_{(4,1,0.42)}$; i.e., VBOC type is II or the second VBOC, $m = p = 4$, $n = 1$, $\alpha = 0.4$. There are four subcarrier periods for every code chip (or transition) equal to 1.955 μs. For every odd signal subcarrier the $+1$ time is equal to 0.342125 μs and the -1 time is equal to 0.146625 μs; even signal subcarrier the $+1$ time is equal to 0.146625 μs and the -1 time is equal to 0.342125 μs. Figure 14 illustrates two periods or chips or code transitions of the BB signal equal to 3.91 μs or 0.48875×8 μs.

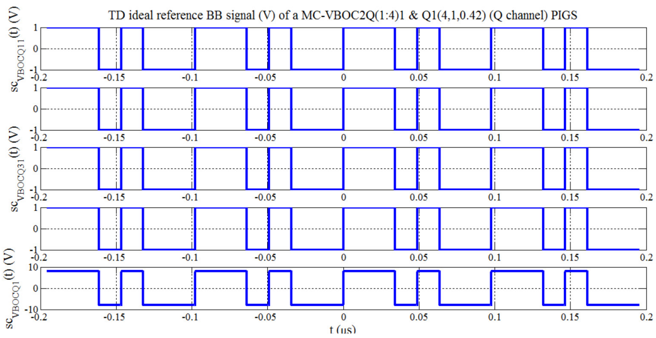

FIGURE 18: 0.4-μs TD reference BB signal of a *MC-VBOC*2Q(1:4)1$_{(4,1,0.42)}$ and *VBOC*2Q$_{(4,1,0.42)}$ PIGS.

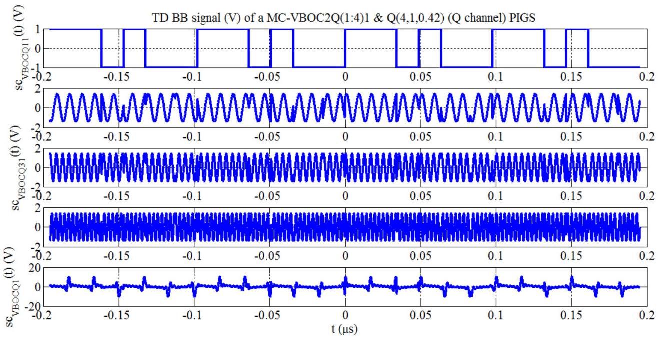

FIGURE 19: 0.4-μs TD BB signal of a *MC-VBOC*2Q(1:4)1$_{(4,1,0.42)}$ and *VBOC*2Q$_{(4,1,0.42)}$ PIGS.

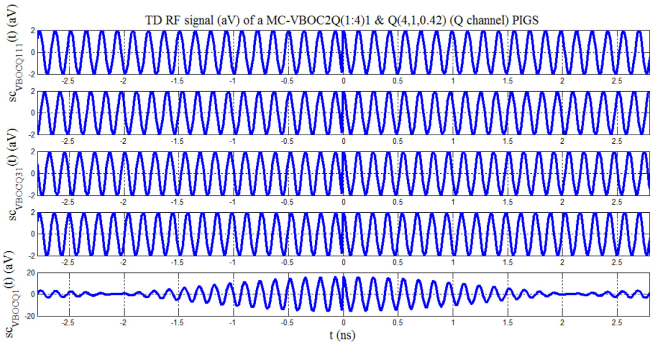

FIGURE 20: 5.5-ns TD RF signal of a *MC-VBOC*2Q(1:4)1$_{(4,1,0.42)}$ and *VBOC*2Q$_{(4,1,0.42)}$ PIGS.

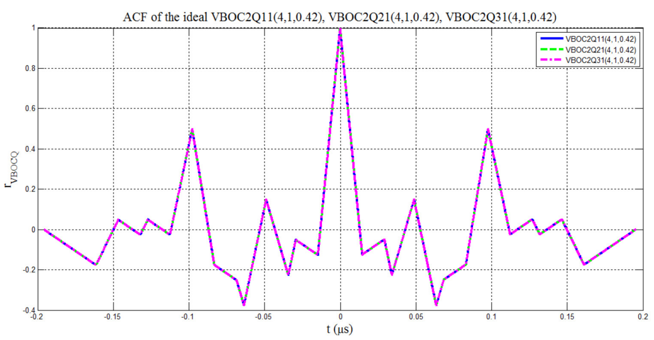

FIGURE 21: 0.4-μs ACF Q Ch: *VBOC*2Q1$_{(4,1,0.42)}$ PIGS.

i.e., period of the subcarrier is equal to 0.48875 μs; and for

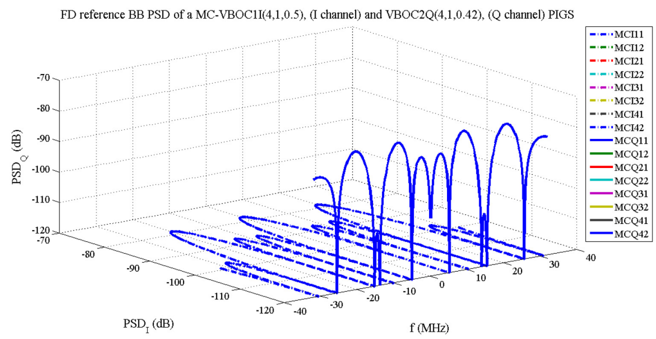

FIGURE 22: 62.5-MHz FD reference BB PSD of a *MC-VBOC*1I$_{(4,1,0.5)}$, (I channel) and *VBOC*2Q$_{(4,1,0.42)}$ (Q channel) PIGS.

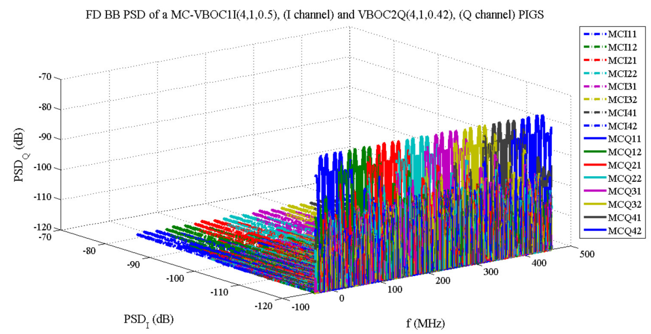

FIGURE 23: 500-MHz FD BB PSD of a *MC-VBOC*1I$_{(4,1,0.5)}$, (I channel) and *VBOC*2Q$_{(4,1,0.42)}$ (Q channel) PIGS.

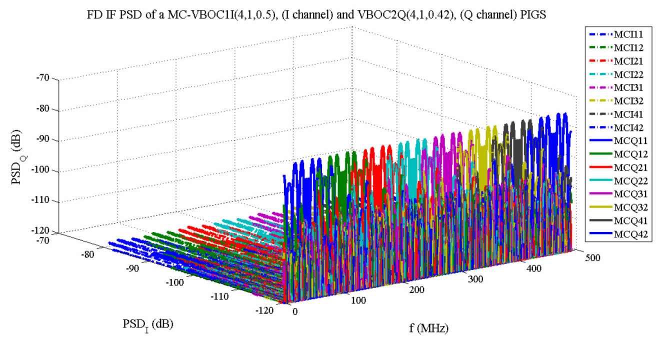

FIGURE 24: 500-MHz FD IF PSD of a *MC-VBOC*1I$_{(4,1,0.5)}$, (I channel) and *VBOC*2Q$_{(4,1,0.42)}$ (Q channel) PIGS.

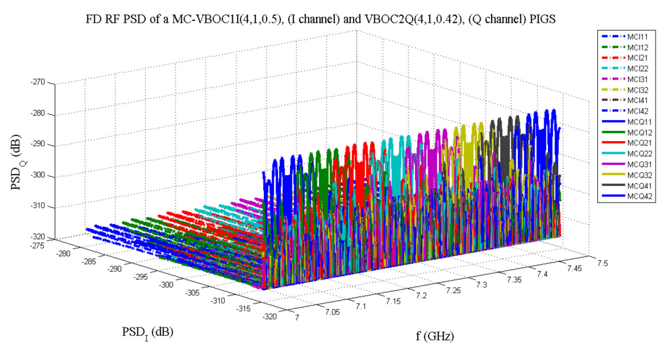

FIGURE 25: 500-MHz FD RF PSD of a *MC-VBOC*1I$_{(4,1,0.5)}$, (I channel) and *VBOC*2Q$_{(4,1,0.42)}$ (Q channel) PIGS the C2-band 7-7.5 GHz.

Figure 19 presents the 0.4-μs TD BB signal of a *MC-* $VBOC2Q(1:4)1_{(4,1,0.42)}$ and $VBOC2Q_{(4,1,0.42)}$, (Q channel) PIGS. Of the four individual transmitter waveforms the top waveform has a subcarrier frequency equal to zero Hz. The second, third, and fourth subcarrier frequencies are 60, 120, and 180 MHz respectively, which is the reason why this type of signal modulation is known as MC-CDMA. Other signal parameters are the same as those in Figure 18.

Figure 20 displays the 5.5-ns TD RF signal of a *MC-* $VBOC2Q11_{(4,1,0.42)}$, $VBOC2Q21_{(4,1,0.42)}$, $VBOC2Q31_{(4,1,0.42)}$, $VBOC2Q41_{(4,1,0.42)}$, and $VBOC2Q_{(4,1,0.42)}$, (Q channel) PIGS. Figure 20 depicts waveforms of Figure 19 unconverted in the C2-band 7-7.5 GHz and because the carrier frequency is so high only the first chip transition is shown.

Figure 21 shows the 0.4-μs ACF Q Ch: $VBOC2Q1_{(4,1,0.42)}$ PIGS. We can see how much the out-of-phase autocorrelation peaks are reduced which is exactly the reason why $VBOC2Q1_{(4,1,0.42)}$ has superior properties compared to $VBOC1I1_{(4,1,0.5)}$. We can see that out-of-phase autocorrelation peaks for $VBOC2Q1_{(4,1,0.42)}$ do not exceed 0.5 as opposed to the out-of-phase autocorrelation peaks for $VBOC1I1_{(4,1,0.5)}$ come as close as 0.75.

The $VBOC2_{(4,1,\alpha)}$ type of modulation reduces the out-of-phase autocorrelation peaks by almost half compared to $VBOC1_{(4,1,\alpha)}$ while at the same time offering a very simple waveform modification. Moreover, the phase of the out-of-phase autocorrelation peaks for $VBOC2_{(4,1,\alpha)}$ is different from the phase of the out-of-phase autocorrelation peaks for $VBOC1_{(4,1,\alpha)}$; i.e., when there is an out-of-phase autocorrelation peak for $VBOC2_{(4,1,\alpha)}$ there is a minimum value of the out-of-phase autocorrelation peaks for $VBOC1_{(4,1,\alpha)}$ and vice versa. Therefore, not only does this type of modulation reduces the number of the out-of-phase autocorrelation peaks but it also offsets them as a function of the type of the VBOC modulation and the parameter of the signal design modulation α.

Figure 22 presents the 62.5-MHz FD reference BB PSD of a *MC-* $VBOC1I_{(4,1,0.5)}$, (I channel) and $VBOC2Q_{(4,1,0.42)}$ (Q channel) PIGS. As illustrated in Figure 22 there are eight $VBOC1I_{(4,1,0.5)}$ PSD in the I channel orthogonal with eight $VBOC2Q_{(4,1,0.42)}$ in the Q channel. There are, however, four transmitters hence every *i*th transmitter contains two $VBOC1Iij_{(4,1,0.5)}$: $VBOC1Ii1_{(4,1,0.5)}$ and $VBOC1Ii2_{(4,1,0.5)}$, for $i = \{1,2,3,4\}$: the transmitter index and $j = \{1,2\}$: the sub-channel index, PSDs in the I channel orthogonal with two $VBOC2Qij_{(4,1,0.42)}$: $VBOC2Qi1_{(4,1,0.42)}$ and $VBOC2Qi2_{(4,1,0.42)}$, for $i = \{1,2,3,4\}$: the transmitter index and $j = \{1,2\}$: the sub-channel index, PSDs in the Q channel which is the reason why this type of signal modulation is known as multicarrier CDMA or MC-CDMA. The maximum values for the PSD for $VBOC2Q1_{(4,1,0.42)}/VBOC1I1_{(4,1,0.5)}$ are $-72/-78$ dB respectively.

Figs. 23, 24 and 25 depict the 500-MHz FD BB/IF/RF PSD of a *C-* $VBOC1I_{(4,1,0.5)}$, (I channel) and $VBOC2Q_{(4,1,0.42)}$ (Q channel) PIGS. The waveforms shown in Figure 23 are exactly the same as the ones shown in Figure 22; however, the only difference is that their IF frequency is shifted in by 40 MHz. The total BB/IF/RF signal bandwidth is 500 MHz which results from 62.5 MHz, the signal bandwidth of either $VBOC1I_{(4,1,0.5)}$ or $VBOC2Q_{(4,1,0.42)}$ waveform, times eight.

Figure 25 shows the 500-MHz FD RF PSD of a *C-* $VBOC1I_{(4,1,0.5)}$, (I channel) and $VBOC2Q_{(4,1,0.42)}$ (Q channel) PIGS the C2-band 7-7.5 GHz. The waveforms shown in Figure 25 are exactly the same as the ones shown in Figure 24; however, the only difference is that their carrier frequency is shifted in by 7 GHz.

This concludes the summary of $VBOC1I_{(4,1,0.5)}$ and $VBOC2Q_{(4,1,0.42)}$ MC-CDMA Simulation Results in C2-band 7-7.5 GHz in which we have illustrated: (1) the waveforms in TD and FD; and (2) ACF in TD and PSD FD.

3-D ACF and PSD simulation results include: (1) 3-D ACF

3.2 3-D ACF and PSD Simulation Results.

3-D ACF and PSD simulation results include: (1) 3-D ACF and PSD $VBOC_{(2,1,\alpha)}(t)$ simulation results and (2) 3-D ACF and PSD $\mathrm{VBOC}_{(4,1,\alpha)}(\mathrm{t})$ simulation results.

3.2.1 3-D ACF and PSD $VBOC_{(2,1,\alpha)}(t)$ Simulation Results

Figure 26 depicts the 0.4-μs 3-D ACF I Ch: $VBOC1I1_{(2,1,\alpha)}(t)$ PIGS. Clearly, from $VBOC1(\alpha)$ examples, we see illustrated the transition of from the ACF of $VBOC1I1_{(2,1,\alpha=0)}(t) = BOC_{(2,1)}(t)$ (left) to the ACF of $VBOC1I1_{(2,1,\alpha=1)}(t) = BOC_{(1,1/2)}(t) = BPSK_0(t)$ (right) as $0 \le \alpha \le 1$.

Figure 27 illustrates the 0.4-μs 3-D ACF Q Ch: $VBOC2Q1_{(2,1,\alpha)}(t)$ PIGS. Clearly, from $VBOC2(\alpha)$ examples, we see illustrated the transition of from the ACF of $VBOC2Q1_{(2,1,\alpha=0)}(t) = BOC_{(2,1)}(t)$ (left) to the ACF of $VBOC2Q1_{(2,1,\alpha=1)}(t) = BOC_{(1,1)}(t)$ (right) as $0 \le \alpha \le 1$.

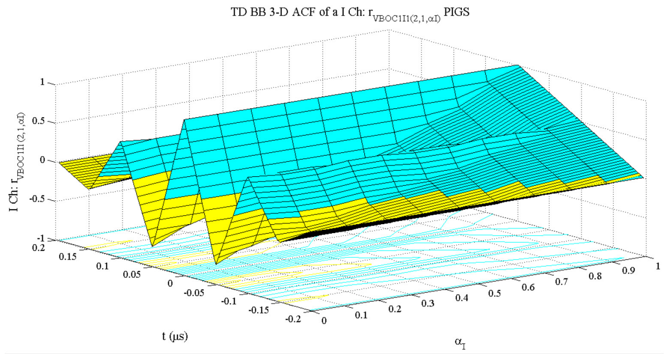

FIGURE 26: 0.4-μs 3-D ACF I Ch: $VBOC1I1_{(2,1,\alpha)}(t)$ PIGS.

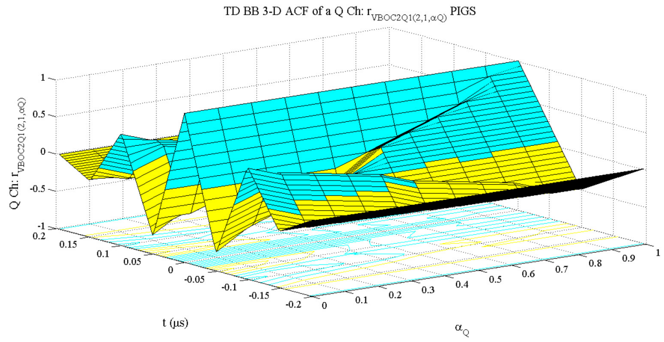

FIGURE 27: 0.4-μs 3-D ACF Q Ch: $VBOC2Q1_{(2,1,\alpha)}(t)$ PIGS.

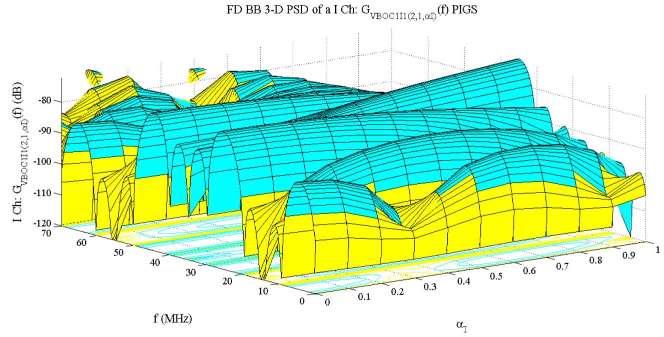

FIGURE 28. 70-MHz FD 3-D PSD I Ch: $VBOC1I1_{(2,1,\alpha)}(t)$, PIGS.

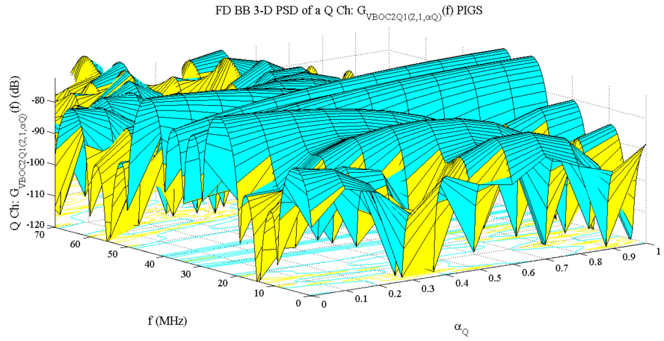

FIGURE 29: 70-MHz FD 3-D PSD, Q Ch: $VBOC2Q1_{(2,1,\alpha)}(t)$ PIGS.

Figure 28 displays the 70-MHz FD 3-D PSD I Ch: $VBOC1I1_{(2,1,\alpha)}(t)$, PIGS. Clearly, from $VBOC1(\alpha)$ examples, we see illustrated the transition of from the PSD of $VBOC1I1_{(2,1,\alpha=0)}(t) = BOC_{(2,1)}(t)$ (left) to the PSD of $VBOC1I1_{(2,1,\alpha=1)}(t) = BOC_{(1,1/2)}(t) = BPSK_0(t)$ (right) as $0 \le \alpha \le 1$.

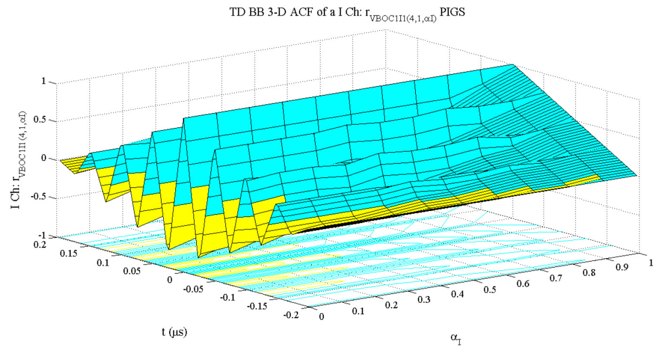

FIGURE 30: 0.4-μs 3-D ACF I Ch: $VBOC1I1_{(4,1,\alpha)}(t)$ PIGS.

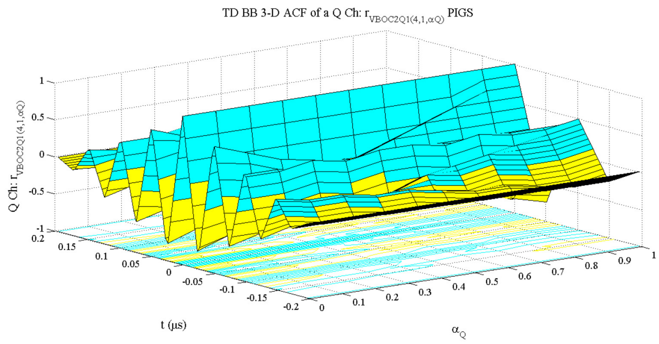

FIGURE 31: 0.4-μs 3-D ACF Q Ch: $VBOC2Q1_{(4,1,\alpha)}(t)$ PIGS.

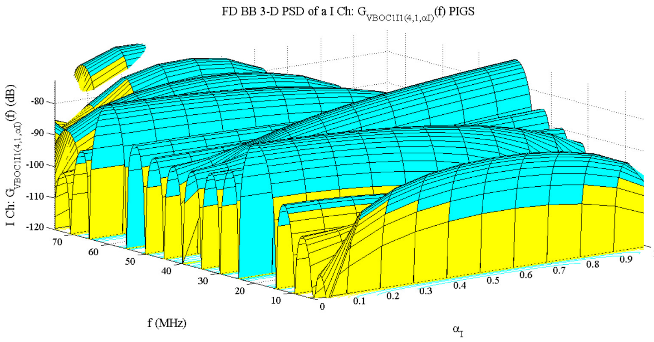

FIGURE 32: 70-MHz FD 3-D PSD I Ch: $VBOC1I1_{(4,1,\alpha)}(t)$, PIGS.

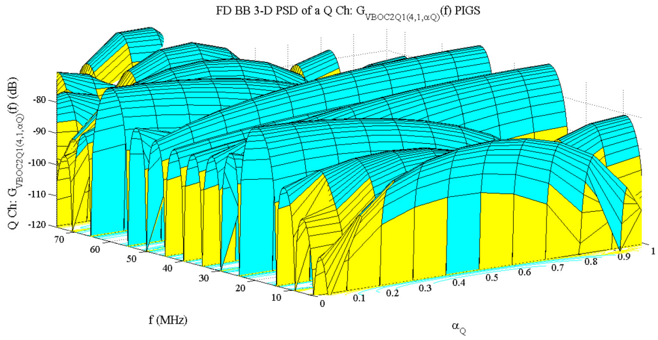

FIGURE 33: 70-MHz FD 3-D PSD, Q Ch: $VBOC2Q1_{(4,1,\alpha)}(t)$ PIGS.

Figure 29 shows the 70-MHz FD 3-D PSD, Q Ch: $VBOC2Q1_{(2,1,\alpha)}(t)$ PIGS. Clearly, from $VBOC2(\alpha)$ examples, we see illustrated the transition of from the PSD of $VBOC2Q1_{(2,1,\alpha=0)}(t) = BOC_{(2,1)}(t)$ (left) to the PSD of $VBOC2Q1_{(2,1,\alpha=1)}(t) = BOC_{(1,1)}(t)$ (right) as $0 \leq \alpha \leq 1$.

3.2.2 3-D ACF and PSD $VBOC_{(4,1,\alpha)}(t)$ Simulation Results

Figure 30 presents the 0.4-µs 3-D ACF I Ch: $VBOC1I1_{(4,1,\alpha)}(t)$ PIGS. Clearly, from $VBOC1(\alpha)$ and ACF definition and discussion, we see illustrated the transition of from the ACF of $VBOC1I1_{(4,1,\alpha=0)}(t) = BOC_{(4,1)}(t)$ (left) to the ACF of $VBOC1I1_{(4,1,\alpha=1)}(t) = BOC_{(1,1/2)}(t) = BPSK_0(t)$ (right) as $0 \leq \alpha \leq 1$.

Figure 31 depicts the 0.4-µs 3-D ACF Q Ch: $VBOC2Q1_{(4,1,\alpha)}(t)$ PIGS. Clearly, from $VBOC2(\alpha)$ exam and ACF definition and discussion, we see illustrated the transition of from the ACF of $VBOC2Q1_{(4,1,\alpha=0)}(t) = BOC_{(4,1)}(t)$ (left) to the ACF of $VBOC2Q1_{(4,1,\alpha=1)}(t) = BOC_{(4,1)}(t)$ (right) as $0 \leq \alpha \leq 1$.

Figure 32 illustrates the 70-MHz FD 3-D PSD I Ch: $VBOC1I1_{(4,1,\alpha)}(t)$, PIGS. Clearly, from $VBOC1(\alpha)$ PSD definition and discussion, we see illustrated the transition of from the PSD of $VBOC1I1_{(4,1,\alpha=0)}(t) = BOC_{(4,1)}(t)$ (left) to the PSD of $VBOC1I1_{(4,1,\alpha=1)}(t) = BOC_{(1,1/2)}(t) = BPSK_0(t)$ (right) as $0 \leq \alpha \leq 1$.

Figure 33 displays the 70-MHz FD 3-D PSD, Q Ch: $VBOC2Q1_{(4,1,\alpha)}(t)$ PIGS. Clearly, from $VBOC2(\alpha)$ examples, we see illustrated the transition of from the PSD of $VBOC2Q1_{(4,1,\alpha=0)}(t) = BOC_{(4,1)}(t)$ (left) to the PSD of $VBOC2Q1_{(4,1,\alpha=1)}(t) = BOC_{(4,1)}(t)$ (right) as $0 \leq \alpha \leq 1$.

Moreover, all the 3-D ACF and PSD waveforms presented in Figs. 26 through 33 are original; i.e., presented for the first time in an ION journal and/or conference paper.

4 Conclusions

This paper is the first complete discussion on pure signal design for the first generation $VBOC2(\alpha, 1-\alpha)$ generalized multidimensional geolocation modulation waveforms.

Contrast the results of this paper with previous signal design methodologies, this paper offers for the first time a complete pure signal design methodology subject to both signal design and optimization parameter α and generalized signal design and optimization parameter p.

Signal parameters α and p not only define the waveform $VBOC2(\alpha, 1-\alpha)$ and generalized ACFs and PSDs but they also play a very important role in the optimization of $VBOC2(\alpha, 1-\alpha)$ generalized ACFs and PSDs. The computational technique offers a unique and original description of the generalized ACFs and PSDs of $VBOC2(\alpha, 1-\alpha)$ as functions of both α and p.

In the paper it is argued that the selection of $BOC(10,5)$ (or the military code or M-Code) on both GPS L1 and L2 frequencies is entirely arbitrary because BOC modulation is a special case of $VBOC2(\alpha, 1-\alpha)$ for $\alpha = 0$ or $\alpha = 1$; hence, all the current state-of-the-art GNSS waveforms exhibit sub-optimal signal design performance even at the end-user when generalized global objective functions are applied.

The above is based on a discussion of $VBOC2(\alpha, 1-\alpha)$ pure signal optimization in [1]: (1) the criteria for validating the closed form expression of the generalized ACF of $VBOC2(\alpha, 1-\alpha)$ known as a set of *continuity theorems*; and (2) the criteria for selecting the optimum $0 \leq \alpha \leq 1$ based on a set of criteria known as *optimization theorems* regardless of generalized parameter p (or subcarrier frequency).

5 Acknowledgement

This work was supported by Giftet Inc. executive office.

6 References

[1] I. Progri, "VBOC1(α) generalized multidimensional geolocation modulation waveforms," *J. Geoloc. GeoInf. Geoint.*, vol. 2015, pp. 19-31, Nov. 2015, DOI: https://doi.org/10.18610/JG3.2015.082101

[2] I. Progri, "VBOC1(α) ACF pure signal optimization," *J. Geoloc. GeoInf. Geoint.*, vol. 2015, pp. 32-43, Nov. 2015, DOI: https://doi.org/10.18610/JG3.2015.082102

[3] I. Progri, "VBOC2(α,1−α) generalized multidimensional geolocation modulation waveforms," *J. Geoloc. GeoInf. Geoint.*, vol. 2015, pp. 44-56, Nov. 2015, DOI: https://doi.org/10.18610/JG3.2015.082103

[4] I. Progri, "VBOC2(α,1−α) ACF pure signal optimization," *J. Geoloc. GeoInf. Geoint.*, vol. 2015, pp. 57-69, Nov. 2015, DOI: https://doi.org/10.18610/JG3.2015.082104

[5] I. Progri, *Indoor Geolocation Systems—Theory and Applications. Vol. I*, 1st ed., Worcester, MA: Giftet Inc., ~800 pp., ~ 2015. (not yet available in print)

[6] I. Progri, "On generalized multi-dimensional geolocation modulation waveforms," in *Proc. IEEE/ION-PLANS 2012*, Myrtle Beach, SC, pp. 919-951, Apr. 2012. DOI: https://doi.org/10.1109/PLANS.2012.6236835

[7] Col. B. Gruber, "GPS directorate: receivers will operate in environments impossible today," *GPS World Mag*., Dec. 1, 2012.

[8] I. Progri, M.C. Bromberg, W.R. Michalson, J. Wang, "A theoretical survey of the spreading modulation of the new GPS signals (L1C, L2C, and L5)," *in Proc. ION-NTM 2007*, San Diego, CA, pp. 561-569, Jan. 2007.

[9] J. Betz, "Something old, something new: signal structures for satellite-based navigation: past, present, and future," *Inside GNSS*, Jul.-Aug. 2013.

[10] D. Davis, "Air Force proposes dramatic redesign for GPS constellation," *Inside GNSS*, May-Jun. 2013.

[11] S.N. Kirillov, V.M. Berdnikov, "Multi-criteria synthesis of signals from satellite navigation systems," *Herald Ryazan State Radio Engineering University* (RSREU), vol. 30, no. 4, 6 pp., 2009.

[12] M.K. Yarlykov, "Correlation functions of single symbols of meander signals in new-generation satellite radio navigation systems," *J. Commun. Tech. Elect.*, vol. 54, no. 8, pp. 912-924, Aug. 2009. DOI: https://doi.org/10.1134/S1064226909080075

[13] V.M. Berdnikov, S.N. Kirillov, "The Analysis of the opportunity of definition of the kind and parameters modulations of navigation signals on the basis of the autocorrelation function," *Herald Ryazan State Radio Engineering University* (RSREU), New Information Technologies in Scientific Researches and Information, XV All-RUSSIA scientific and Technical Conference of Students, Young Scientists and Experts, Ryazan, pp. 130-132, 2010. (in Russian)

[14] J.W. Betz, "Binary offset carrier modulation for radionavigation," *Navigation*, vol. 48, no. 4, pp. 227-246, winter 2001-2002. DOI: https://doi.org/10.1002/j.2161-4296.2001.tb00247.x

[15] J. Betz, C.R. Cahn, P.A. Dafesh, C.J. Hegarty, K.W. Hudnut, A.J. Jones, R. Keegan, K. Kovach, L.S. Lenahan, H.H. Ma, J.J. Rushanan, T.A. Stansell, C.C. Wang, S.K. Yi, "L1C signal design options," in *Proc. 2006 Nat. Tech. Mtg. ION*, Monterey, CA, pp. 685-697, Jan. 2006.

[16] G.W. Hein, J.-A. Avila-Rodriguez, S. Wallner, A.R. Pratt, J. Owen, J.-L. Issler, J.W. Betz, C.J. Hegarty, S. Lenahan, J.J. Rushanan, A.L. Kraay, T.A. Stansell, "MBOC: the new optimized spreading modulation recommended for GALILEO L1 OS and GPS L1C," in *Proc. IEEE/ION PLANS 2006*, San Diego, CA, pp. 883-892, Apr. 2006. DOI: https://doi.org/10.1109/PLANS.2006.1650688

[17] J. Betz, M.A. Blanco, C.R. Cahn, P.A .Dafesh, C.J. Hegarty, K.W. Hudnut, V. Kasemsri, R. Keegan, K. Kovach, L.S. Lenahan, H.H. Ma, J.J. Rushanan, D. Sklar, T.A. Stansell, C.C. Wang, S.K. Yi, "Description of the L1C signal," in *Proc. 19th Inter. Tech. Mtg. Sat. Div. ION (ION GNSS 2006)*, Fort Worth, TX, pp. 2080-2091, Sep. 2006.

[18] T. Stansell, K.W. Hudnut, R.G. Keegan, "GPS L1C: enhanced performance, receiver design suggestions, and key contributions," in *Proc. 23rd Inter. Tech. Mtg. Sat. Div. ION (ION GNSS 2010)*, Portland, OR, pp. 2860-2873, Sep. 2010.

[19] J.-A. Avila-Rodriguez, S. Wallner, G.W. Hein, B. Eissfeller, M. Irsigler, J.-L. Issler, "A vision on new frequencies, signals and concepts for future GNSS systems," in *Proc. 20th Inter. Tech. Mtg. Sat. Div. ION (ION GNSS 2007)*, Fort Worth, TX, pp. 517-534, Sept. 2007.

[20] Anon., "GLONASS Navigational radio-signal in bands L1, L2," Russian Institute of Space Device Engineering, Moscow, Russia, 2008.

[21] J.A. Avila-Rodriguez, "On generalized signal waveforms for satellite navigation," *Ph.D. Dissertation*, University FAF Munich, Neubiberg, Germany, 408 pp., June 2008.

[22] S. Revnivykh, "GLONASS status and progress," in *Proc. 23rd Inter. Tech. Mtg. Sat. Div. ION (ION GNSS 2010)*, Portland, OR, pp. 609-633, Sep. 2010.

[23] J.-A. Avila-Rodriguez, G.W. Hein, S. Wallner, J.-L. Issler, L. Ries, L. Lestarquit, A. de Latour, J. Godet, F. Bastide, T. Pratt, J. Owen, "The MBOC modulation: the final touch to the Galileo frequency and signal plan," *Navigation*, vol. 55, no. 1, pp. 14-28, spring 2008. DOI: https://doi.org/10.1002/j.2161-4296.2008.tb00415.x

[24] L. Lestarquit, G. Artaud, J.-L. Issler, "AltBOC for dummies or everything you always wanted to know about AltBOC," in *Proc. 21st Inter. Tech. Mtg. Sat. Div. ION (ION GNSS 2008)*, Savannah, GA, pp. 961-970, Sep. 2008.

[25] T. Pratt, "Frequency diversity or no frequency diversity," *Proc. 23rd Inter. Tech. Mtg. Sat. Div. ION (ION GNSS 2010)*, Portland, OR, pp. 3021-3040, Sep. 2010.

[26] J.-A. Avila-Rodriguez, S. Wallner, J.-H. Won, B. Eissfeller, A. Schmitz-Peiffer, J.-J. Floch, E. Colzi, J.-L. Gerner, "Study on a Galileo signal and service plan for C-band," in *Proc. 21st Inter. Tech. Mtg. Sat. Div. ION (ION GNSS 2008)*, Savannah, GA, pp. 2515-2529, Sep. 2008.

[27] F.M.G. Sousa, F.D. Nunes "New expressions for the autocorrelation function of BOC GNSS signals," *Navigation*, vol. 60, no. 1, pp. 1-9, spring 2013. DOI: https://doi.org/10.1002/navi.30

[28] I. Progri, M.C. Bromberg, W.R. Michalson, "Maximum likelihood GPS parameter estimation," *Navigation*, vol. 52, no. 4, pp. 229-238, winter 2005-2006. DOI: https://doi.org/10.1002/j.2161-4296.2005.tb00365.x

[29] I. Progri, M.C. Bromberg, J. Wang, "Markov Chain, Monte Carlo global search and integration for Bayesian, GPS, parameter estimation," *Navigation*, vol. 56, no. 3, pp. 195-204, fall 2009. DOI: https://doi.org/10.1002/j.2161-4296.2009.tb01755.x

[30] W.R. Michalson, I. Progri, "Reconfigurable geolocation system," US Patent 7,079,025, July 2006.

[31] I.F. Progri, "An assessment of indoor geolocation systems," *Ph.D. Dissertation*, Worcester Polytechnic Institute, May 2003.

[32] I. Progri, J.M. Hill, W.R. Michalson, "An investigation of the pseudolite's signal structure for indoor applications," in *Proc. ION-AM 2001*, Albuquerque, NM, pp. 453-462, June 2001.

[33] I. Progri, W.R. Michalson, "The impact of proposed pseudolite's signal structure on the receiver's phase and code error," in *Proc. ION-AM 2001*, Albuquerque, NM, pp. 414-422, June 2001.

[34] I. Progri, W.R. Michalson, "An alternative approach to multipath and near-far problem for indoor geolocation systems," in *Proc. 14th Inter. Tech. Mtg. Sat. Div. ION (ION GPS 2001)*, Salt Lake City, UT, pp. 1434-1443, Sep. 2001.

[35] I. Progri, W.R. Michalson, J. Wang, M.C. Bromberg, R.J. Duckworth, "Requirements of a C-CDMA pseudolite indoor geolocation system," *in Proc. ION-AM 2007*, Cambridge, MA, pp. 654-658, Apr. 2007.

[36] I. Progri, W.R. Michalson, J. Wang, M.C. Bromberg, "Indoor geolocation using FCDMA pseudolites: signal structure and performance analysis," *Navigation*, vol. 54, no. 3, pp. 242-256, fall 2007. DOI: https://doi.org/10.1002/j.2161-4296.2007.tb00407.x

[37] I. Progri, *Geolocation of RF Signals—Principles and Simulations*. 1st ed., New York, NY: Springer SBM, LLC, 330 pp., Jan. 2011. DOI: https://doi.org/10.1007/978-1-4419-7952-0